INTEGRAL

Science Operations Centre

Announcement of Opportunity for Observing Proposals

OMC Observer's Manual

INTG-AO-00033

Issue 1.0

17 February 2021

Maintained by

Jan-Uwe Ness

This page was intentionally left blank

Contributors to this manual include:

J. M. Mas-Hesse, OMC PI, CAB-CSIC/INTA,

A. Domingo, OMC team, CAB-CSIC/INTA (author)

J. Alfonso-Garzón, OMC team, CAB-CSIC/INTA

E. Kuulkers, ISOC, ESA/ESAC

P. Kretschmar, ISOC, ESA/ESAC

G. Belanger, ISOC, ESA/ESAC

J.U. Ness (maintainer)

Table of Contents

This page was intentionally left blank

1 Introduction

The Optical Monitoring Camera (OMC) is a wide-field optical instrument using a large-format CCD detector, limited by a relatively low telemetry rate. It measures the optical emission from the prime targets of the two gamma-ray instruments SPI and IBIS. The OMC offers the first opportunity to make observations of long duration in the optical band simultaneously with those at hard X-rays and gamma-rays. Multi-band observations are particularly important in high-energy astrophysics where variability is typically rapid, unpredictable and of large amplitude. The main objectives of the OMC can be summarised as follows:

- To monitor during extended periods of time the optical emission of all high-energy targets within its field of view, simultaneously with the high-energy instruments.

- To provide simultaneous and calibrated standard V-band photometry of the high-energy sources to allow comparison of their high-energy behaviour with previous or future ground-based optical measurements.

- To analyse and locate the optical counterparts of high-energy transients detected by the other instruments, especially gamma-ray transients.

- To monitor any other optically variable sources serendipitously within the OMC field of view, which may require long periods of continuous observations in order to understand their underlying physics (variable stars, flaring and eruptive objects, etc.).

The purpose of this manual is to present all the information about the OMC which is necessary for the preparation of INTEGRAL proposals. We refer the interested reader to a sequence of papers on the OMC payload in the A&A special INTEGRAL issue (2003, Vol. 411, L261-L289). This issue also contains various other papers on the first results from in-flight observations. A more detailed description of the instrument performances can be found in the OMC Analysis Scientific Validation Report (http://www.isdc.unige.ch/integral/analysis), part of the Off-line Scientific Analysis (OSA) documentation.

Figure 1: OMC Flight model.

Table 1: OMC parameters and scientific performances.

Parameter	In-orbit value
Field of view	$4.979° \times 4.979°$
Aperture	5 cm diameter
Focal length	153.7 mm (f/3.1)
Optical throughput	> 70% at 550 nm
Stray light reduction factor[1]	$<< 10^{-4}$
Angular resolution	≈ 23" Gaussian PSF (FWHM=1.3±0.1 pix)
Point source location accuracy	≈ 2"
Angular pixel size	17.504" × 17.504"
CCD pixels	2061×1056 (1024×1024 image area) ($13 \times 13 \ \mu m^2$ per pixel)
CCD Quantum efficiency	88% at 550 nm
CCD full well capacity	~120000 electrons/pixel
ADC levels	12 bit signal, 4096 levels: ~30 cts/digital level (low gain) ~5 cts/digital level (high gain)
Frame transfer time	≈ 2 ms
Time resolution	> 3 s
Typical integration times	10s – 50s – 200s
Wavelength range	Johnson V filter (centred at 550 nm)
Limit magnitude (10 × 200 s, 3σ) (50 × 200 s, 3σ) (100 × 200 s, 3σ)	18.1 (m_V) 18.9 (m_V) 19.3 (m_V)
Sensitivity to variations (10 × 100 s, 3σ)	$\Delta m_V < 0.1$, for $m_V < 16$

---

[1]This parameter defines the factor by which the flux from any source outside the FOV is reduced by multiple reflections before reaching the detector surface as background light. The stray light from sources at >10° from the optical axis is negligible.
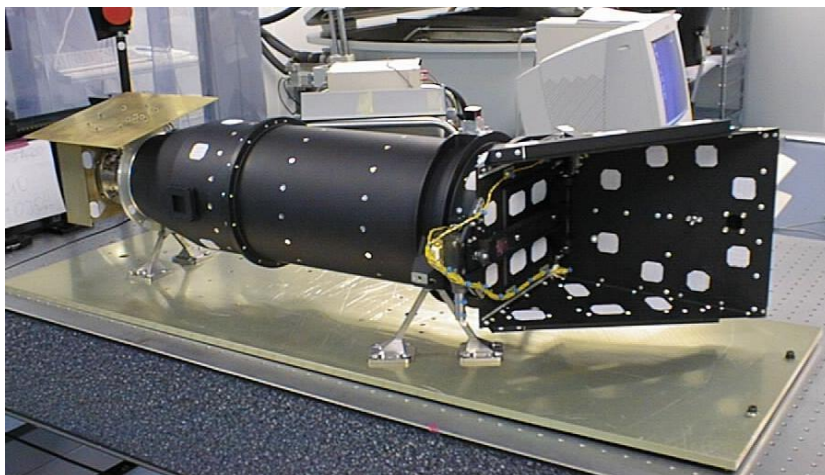
2 Description of the instrument

2.1 Overall design

The OMC consists of an optical system focused onto a CCD detector. The optics is refractive with an entrance aperture of 5 cm diameter and a square field of view of about 5°×5°. A Johnson V filter allows photometric calibration in a standard system. An optical baffle ensures the necessary reduction of scattered sunlight and also of the unwanted stray-light coming from non-solar sources outside the field-of-view (FOV). A deployable cover protected the optics from contamination during ground operations and early operations in orbit. It was released during the first steps of the commissioning phase. It now forms part of the baffle. See Figure 1 for a picture of the flight model and Figure 2 for a diagram of the OMC.

The camera unit is based on a large-format CCD (2061×1056 pixels) working in frame transfer mode (1024×1024 image area and 1024×1024 storage area, not exposed to light). This design, with a frame transfer time of around 2 ms, allows continuous measurements and makes it unnecessary to have a mechanical shutter. A LED light source within the optical cavity provides "flat-field" illumination of the CCD to calibrate the relative sensitivities of the pixels.

2.2 The optics

The optical system, as shown in Figure 3, consists of:

- a 6-fold lens system composed of two different types of radiation resistant glass,

- a filter assembly; the Johnson V filter has been defined with a combination of 2 different filters,

- a lens barrel giving mechanical support to the lenses and ensuring their alignment.

2.3 The CCD detector

Figure 2: A 3-D cut of the OMC Camera Unit.

The full well capacity is the maximum number of counts measurable per single pixel, which in the case of OMC is ≈ 120 000 cts. This parameter critically determines the dynamic range of the
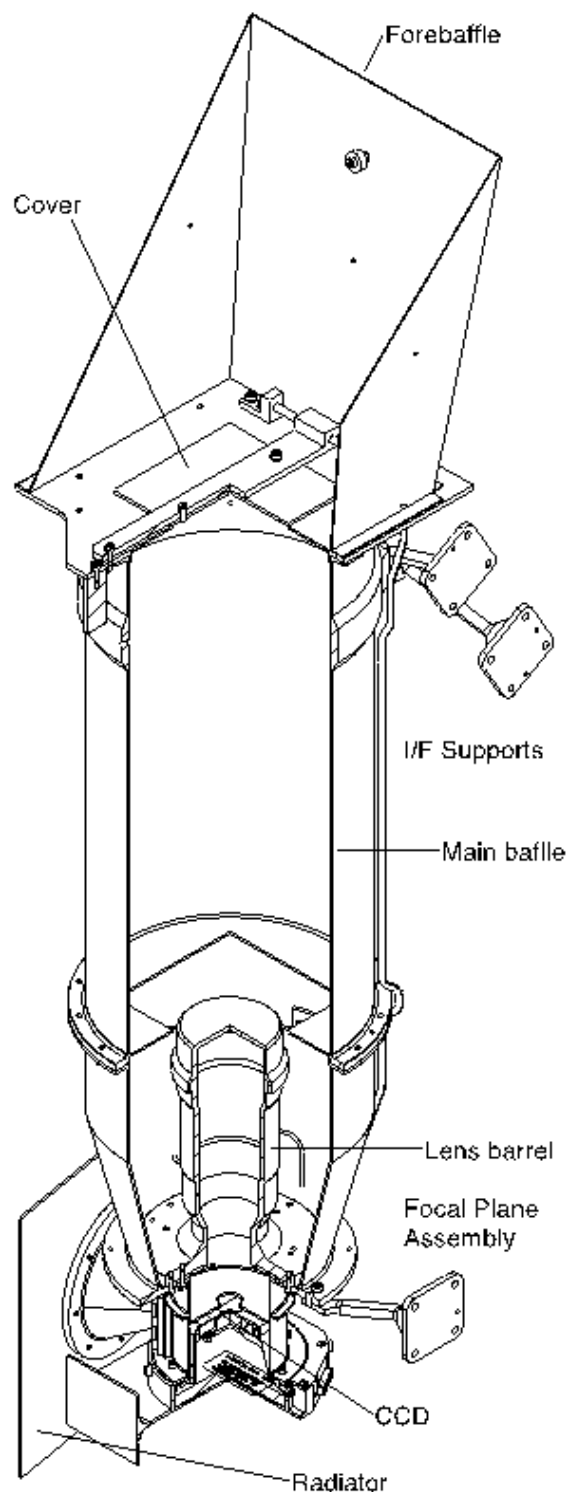
detector. The Analogue to Digital Converters (ADCs) used in the OMC have the capability of digitizing the analogue signal coming from the CCD read-out ports to 12 bits, i.e., they provide a discrete output in up to 4096 digital levels. The ADCs are operated with 2 gain values. At the standard low gain, the full dynamic range of the CCD, 0 to 120 000 cts per pixel, is digitized into 0 to 4095 Digital Levels (DN), at a linear scale of ≈ 30 cts/DN. At high gain, which is currently used only during calibration, only the 0 to 20 000 cts per pixel range is digitized into 0 to 4095 DN, with ≈ 5 cts/DN. This allows a more accurate photometry in some cases down to approximately the noise limit of the CCD. Finally, the CCD is cooled by means of a passive radiator (illustrated in Figure 2) to an operational temperature of around $-80°$ C.
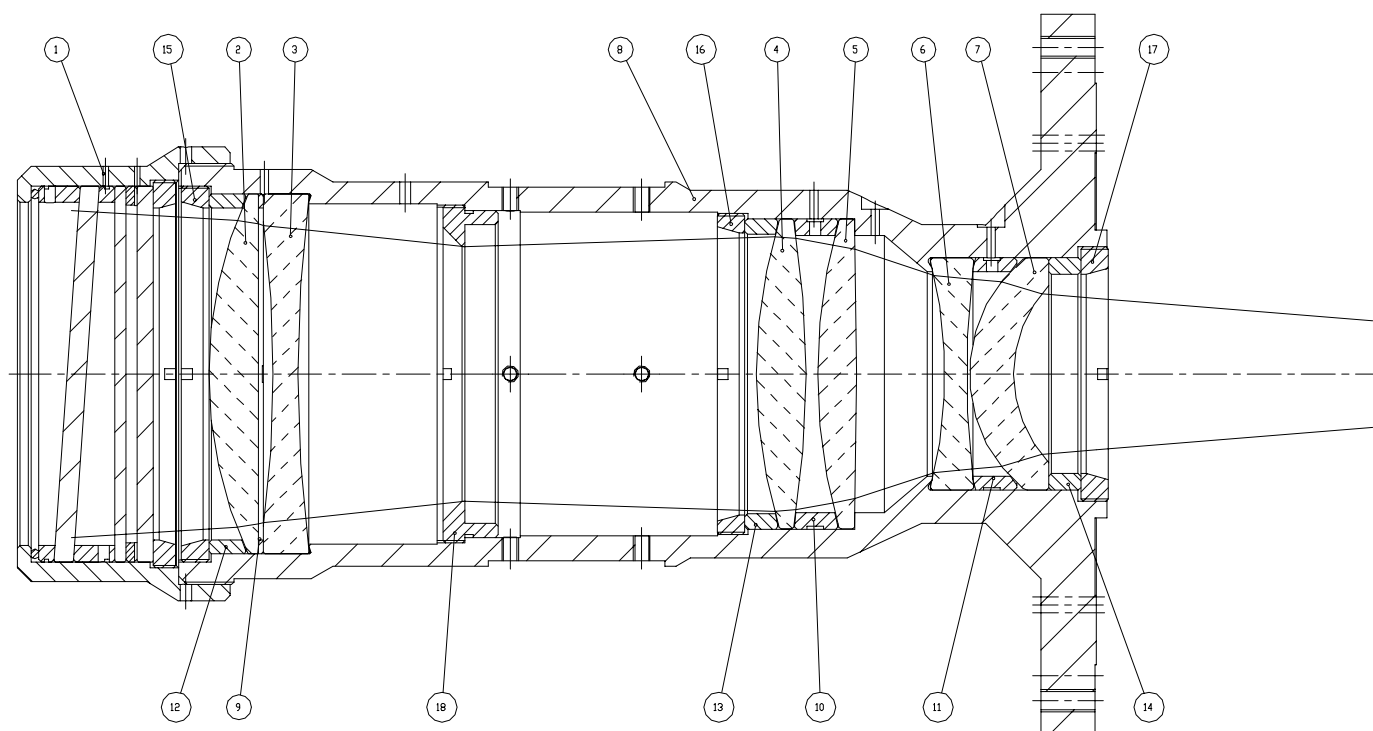

Figure 3: Optical system layout. 1: filter assembly housing; 2-7: lenses; 8: lens barrel; 9-14: spacers; 15-17: retainers; 18: aperture stop.

3 Instrument operations

Because of telemetry constraints (only ≈ 2.2 kbps are allocated to the OMC) it is not possible to transmit the entire OMC image to the ground. For this reason windows are selected around the proposed main gamma-ray target as well as other targets of interest in the same field of view. The observers obtain the data pertinent to their target, as well as all the other OMC CCD sub-windows taken during the observation (see also the **Overview, Policies and Procedures** document). These additional targets are automatically selected from the OMC "Input Catalogue". Two observation modes are available to the observer: the normal and the fast monitoring modes.

3.1 Normal science operations mode

In the normal science operations mode, the OMC monitors the optical flux of a number of targets, including the high-energy sources within its FOV, other sources of interest, stars for photometrical calibration and masked pixels from the CCD to monitor the dark current and bias. Variable integration times during a pointing allow the monitoring of both bright and faint sources. Operations are performed automatically in the following way:

- The observing sequence starts by obtaining a series of images of 10 "astrometric" reference stars, spread over the field of view. This makes it possible to calculate on-board the pointing of the OMC optical axis with accuracy better than 0.5 pixels ($\approx 9''$).

- Then a set of photometric stars is observed (10 stars in the field of view with good photometric quality).

- The CCD, centred in a target field, is then exposed with the following sequence of integration times: 10 s – 50 s – 200 s. After each exposure the full frame is transferred to the occulted part of the chip and the next integration starts. An optimum use of the CCD, from the point of view of the noise (read-out and cosmic rays), is obtained for integration times of around 200 s, so that for the faintest objects several exposures of 200 s are summed during the analysis on ground. The number of integrations that can be added depends on the time during which the spacecraft keeps the same pointing without dithering (typically 30 minutes). The brightest stars will saturate their corresponding pixels for such integration times, but the combination of short and long exposures allows one to increase the magnitude range for a given field.

- A number of windows (of typically 11×11 pixels, or $\approx 3'\times3'$) are extracted around each object of interest and transmitted to the ground (see, e.g. Figure 4). When using the Proposal Generation Tool (PGT, see the **Overview, Policies and Procedures** document) observers may specify a "Monitoring Window Size" for their target. The maximum allowed value is 30′, corresponding to a $\approx 30'\times30'$ square window. Any value smaller than 3′ will, in fact, be executed with a 3′×3′ window. Values greater than 3′×3′ are executed as a mosaic of smaller windows, e.g. several 3′×3′ windows, piled side by side, which will have to be recombined on ground. Large window sizes can be useful for targets without precise, optically measured coordinates (see, e.g. Figure 5). See also Section 5.2.
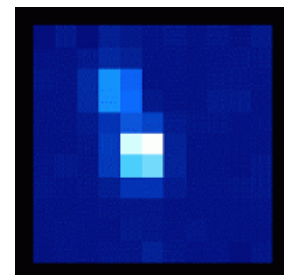

Figure 4: OMC sub-window of 11 × 11 pixels.

- Continuous monitoring of the central target with OMC will only be possible if the dithering pattern selected in the Proposal Generation Tool is none (staring) or hexagonal (see the **Observation Tools Software User Manual** document). In the case of larger dithering patterns, like the 5×5 one, the target will fall within the OMC field of view only for a fraction of the pointings.
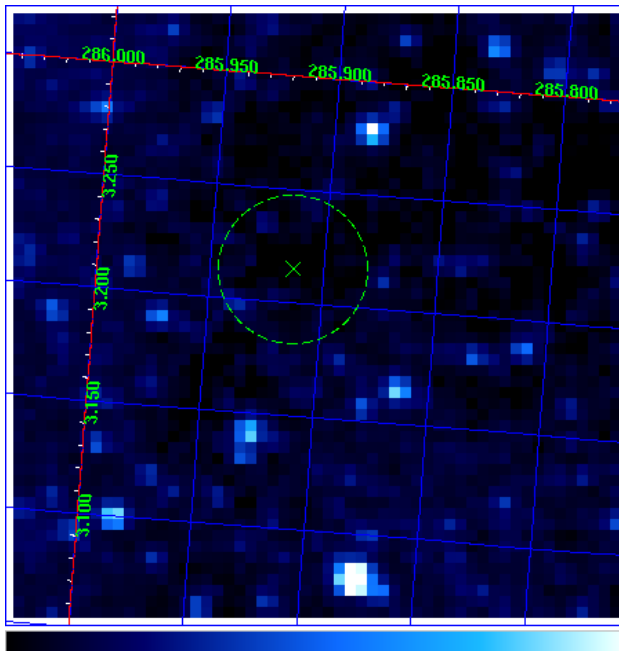

Figure 5: This image corresponds to the High Mass X-ray Binary 4U 1901+03, which generated a mosaic of 5×5 OMC sub-windows (16'×16'). The green cross and circle are, respectively, the position and positional error of 4U 1901+03 in the IBIS catalogue.

3.2 Fast monitoring mode

In the normal mode it is not possible to perform a continuous monitoring with a time resolution finer than 10 seconds. Therefore, when fast variability is expected, the fast monitoring mode should be chosen. With this mode, integrations of 3 seconds are performed at intervals of 4.5 seconds and only the sections of the CCD containing the target of interest are read from the CCD and transmitted. This implies that the position of the source must be known with accuracy better than the window size used for fast monitoring (11×11 pixels, i.e. $3' \times 3'$), and that the source is bright enough to be monitored with integration times below 10 s (see also Figure 11).

On the other hand, note that this mode should be selected for any target brighter than V = 7.5 and fainter than V = 5.0 to avoid saturation of the CCD, whatever kind of variability is expected. Targets brighter than V = 5.0 are too bright for the OMC, even with integrations of 3 seconds; nothing can be done in that case: the source will then saturate the CCD.

3.3 The OMC input catalogue

As explained above, besides the proposed target(s), the OMC observes astrometric and photometric stars and other targets of scientific interest within its field of view at a given time. For this purpose, a catalogue has been compiled by the OMC team containing over 540 000 sources. It can be down-loaded by FTP (**ftp://ftp.cab.inta-csic.es/pub/integral/catalogue/**) and a search form is also available (**http://sdc.cab.inta-csic.es/omc/**).

The input catalogue includes:
- Known optical counterparts of gamma-ray sources.
- Known optical counterparts of X-ray sources.
- X-ray sources detected and catalogued by ROSAT.
- Quasars observable with the OMC.
- Additional known AGNs.
- Known eruptive variable stars (including novae and cataclysmics).
- Variable objects which may require additional optical monitoring.
- HIPPARCOS reference stars for positioning and photometrical calibration.

During the mission, additional sources of interest are added to the catalogue, namely:
- Newly discovered optical counterparts of high-energy sources.
- Regions of special interest for INTEGRAL science.
- New supernovae.
- New eruptive variable stars.
- Any other Target of Opportunity (TOO).

For every scheduled observation, the coordinates of all the targets of interest within the corresponding field of view are extracted from the OMC input catalogue. The table of targets of interest is included in the telecommands to be sent to the OMC before any new pointing, allowing the observer to identify all downloaded CCD windows.

3.4 Gamma-ray bursts and transient sources

The INTEGRAL Burst Alert System (IBAS) is located at the INTEGRAL Science Data Centre (ISDC) near Geneva. IBAS searches for gamma-ray bursts (GRB) using SPI/ACS triggers and IBIS/ISGRI detections and position measurements. If IBAS detects a GRB and it is within the OMC FOV, a near-real-time command is sent to the OMC, via the INTEGRAL Mission Operations Centre (MOC), located in Darmstadt. Upon reception of this telecommand, the OMC stops the observations planned for this pointing and starts to monitor a single window of 91×91 pixels ($\approx 24' \times 24'$) around the region where the burst has been detected, with a fixed integration time of 100 s. This "trigger" mode is active during the rest of the pointing. The expected delay between the start of the burst and the start of OMC monitoring is less than 1 minute. Specifically, the OMC monitoring starts less than 15 seconds after the IBAS trigger. This makes it possible to obtain slightly delayed but simultaneous optical, X-ray and gamma-ray data of any burst taking place within the OMC FOV.

The **Overview, Policies and Procedures** document describes how and under which conditions the OMC data are distributed to the observers in the case of a gamma-ray burst or a transient.

Based on CGRO/BATSE observations, around one GRB per year was expected within the OMC field of view. Nevertheless, up to now the OMC has had only two GRBs in its field of view, on July 26th, 2005 and January 18th, 2012. Unfortunately, the first one (GRB 050626) was very close to Alpha Crucis, a very bright star (V = 0.8 mag), which saturated completely the CCD and hit the optical counterpart of the CCD, as shown in the image in Figure 6. For the second one (XRF 120118A) the OMC, starting the observations only 45 s after the XRF, did not detect any coincident new source brighter than V = 17.7 mag (see Figure 7).
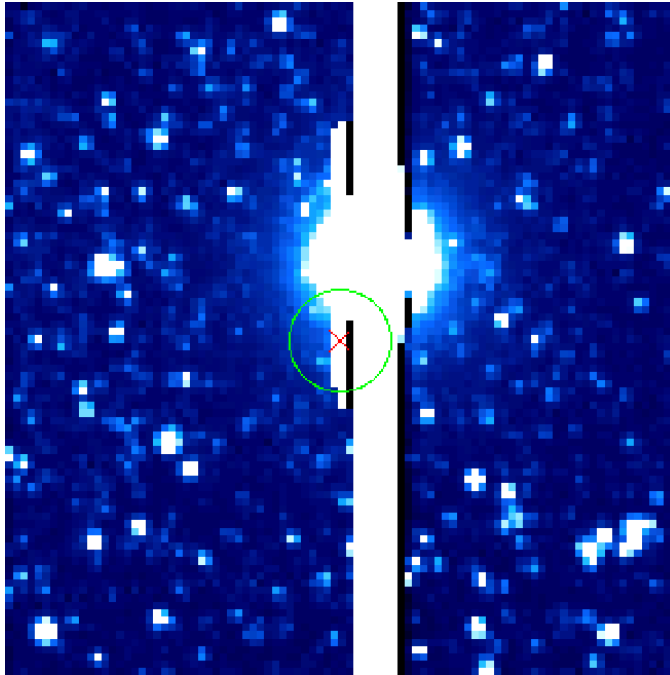
Figure 6: The first GRB which occurred in the field of view of the OMC, on 2005 July 26 (GRB 050626). The red cross marks the position of the GRB, within the error circle in green. Unfortunately, the GRB happened to be close to a very bright, 0.8 magnitude in V, star (Alpha Crucis). The bright star completely saturated the CCD, causing the white vertical strip, and therefore completely contaminating the GRB emission.
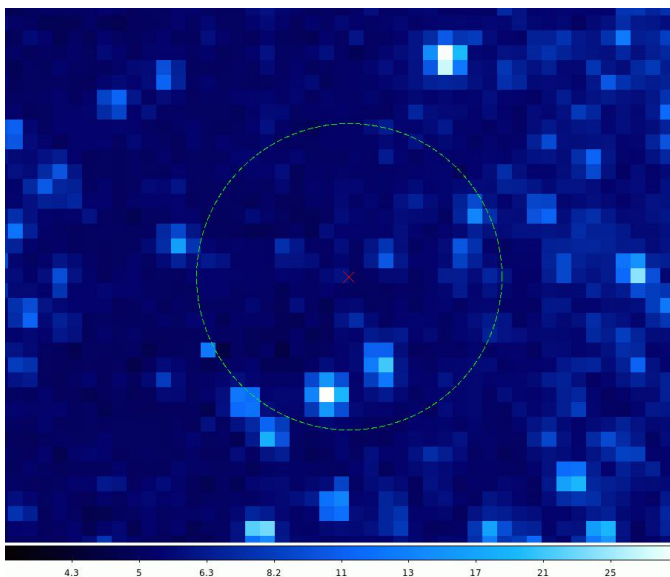

Figure 7: OMC image of the X-Ray Flash detected by INTEGRAL on 2012 January 18 (XRF 120118A). The red cross marks the position of the XRF, within the error circle in green. OMC did not detect any new source brighter than V = 17.7 mag inside the XRF error circle.

4 Instrument performances

4.1 Background and read-out noise

There are two main sources of background flux for the OMC, both related to the rather large angular pixel size of $17.5'' \times 17.5''$: scattered sunlight (zodiacal light) and unresolved stellar sources. Maximum background conditions correspond to pointings towards the galactic plane with maximum zodiacal light, while the minimum background is achieved around the galactic pole with minimum zodiacal light.
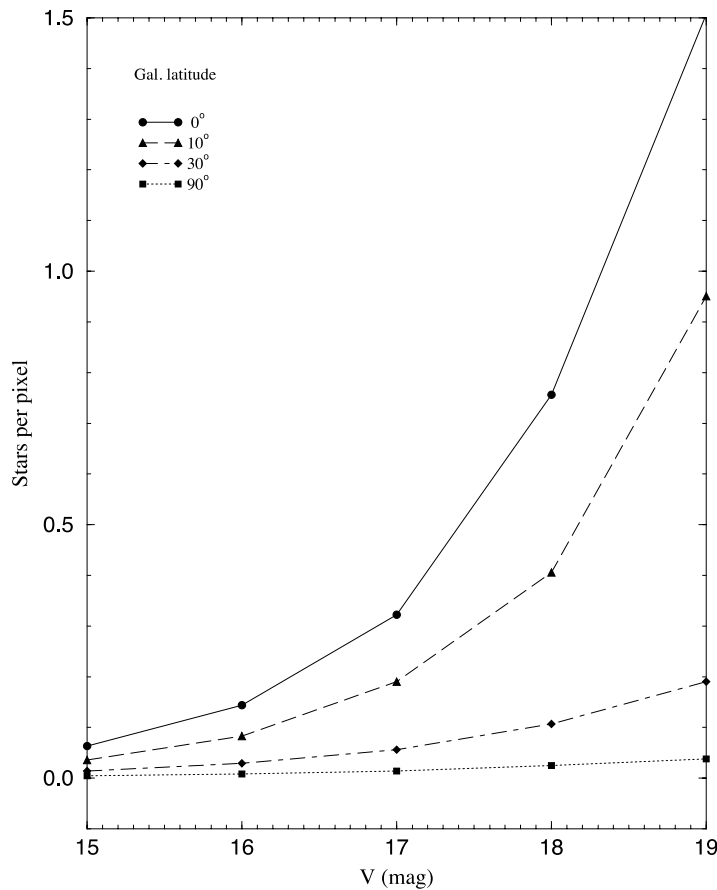

Figure 8: Average number of stars per pixel brighter than a given V magnitude at different galactic latitudes.

Figure 8 shows the average number of stars brighter than a given magnitude contained within a single OMC pixel. It can be seen that, on average, source confusion does not occur for objects brighter than $m_V = 17$ at any galactic latitude. For $m_V = 18.0$ source confusion can become problematic in some regions very close to the galactic plane.

It is important to stress that on the galactic plane there are on average more than one star per pixel with m_V between 17 and 19. The density of stars on the galactic plane indeed determines the limiting magnitude of the instrument. At galactic latitudes $|b| > 30°$ the problem of source confusion becomes negligible, except for specific cases in which bright stars are separated by just a few arcsec. The background measured in orbit corresponds well to the expected values.

The read-out noise of the OMC as measured on ground is between 1-1.5 DN/pixel (digital levels) for low gain and between 3-3.5 DN/pixel in high gain, corresponding to 30-45 cts and 15-17 cts, respectively. The read-out noise measured in orbit is consistent with these values.

4.2 Limiting faint magnitude

Assuming a minimum level of background (see the definition in the previous section) and a combination of 10 exposures of 200 s each, the limiting magnitude of the OMC is found to be $m_V = 18.1$ (3σ detection level). This value corresponds to a limiting sensitivity of the instrument of 2.1×10^{-16} erg cm^{-2} s^{-1} Å^{-1} or, alternatively, 5.8×10^{-5} ph cm^{-2} s^{-1} Å^{-1}, at 550 nm. At a maximum background level (as defined above) the limiting magnitude is $m_V = 17.5$. Note that these sensitivities can only be achieved for isolated stars for which the background can be properly estimated. Figure 9 shows the limiting faint magnitude for both maximum and minimum background as a function of integration time, assuming in all cases that 10 images have been combined to increase the signal to noise ratio. Figure 10 shows the limiting magnitude in best background conditions, and for different combinations of exposures.

Measurements in orbit show that the OMC is on average about 30% more sensitive than estimated during ground-based calibrations. However, the absolute photometric calibration changes with time and is continuously updated by the OMC team. Currently, about every 16th revolution a dedicated OMC flat field and dark current calibration observation is carried out.
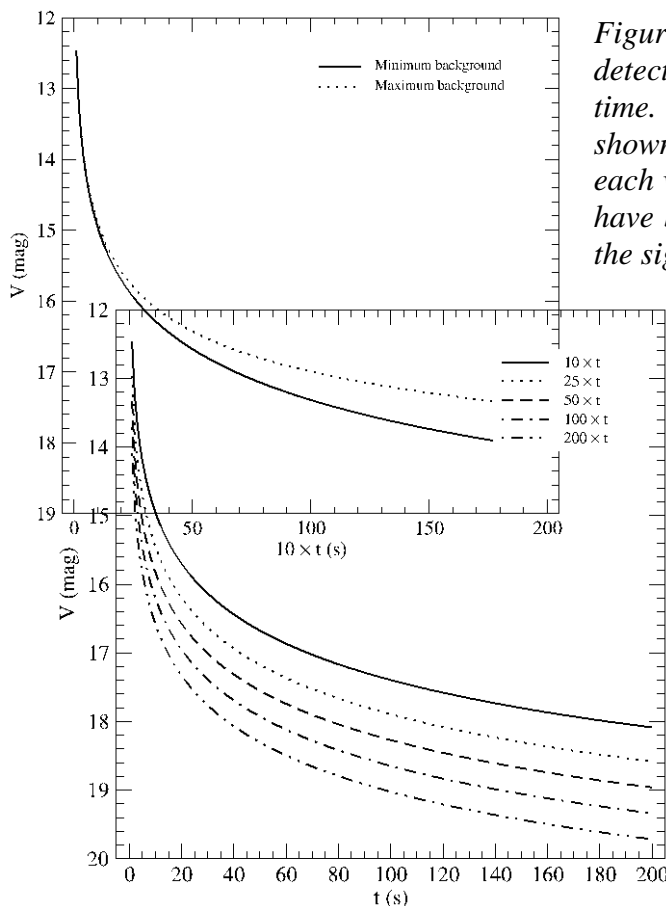

Figure 9: Limiting faint magnitude for a 3σ detection in the V band as a function of integration time. The best and the worst background cases are shown. It is assumed that 10 separate exposures, each with the integration time as given in the plot, have been combined together in order to increase the signal to noise ratio.

Figure 10: As Figure 9. Best case background conditions are assumed (galactic pole, no zodiacal light). The curves correspond to different total numbers of images being combined.

4.3 Limiting bright magnitude

The full well capacity of the CCD constrains the magnitude of the brightest stars that can be measured without pixel saturation for a given integration time. With 10 s integrations, the central pixel becomes saturated for objects brighter than $m_V = 7$. With integrations of 200 s, even stars with $m_V \approx 10$ will start to saturate the

CCD. Severe saturation of the CCD might imply losing the information from the surrounding pixels and potentially from the column containing the source, but no damage is expected on the detector.

Figure 11 shows the predicted number of counts on the CCD as a function of V magnitude for a 10 s integration. This number corresponds to the counts expected in the central (brightest) pixel only. Finally, Figure 12 gives the integration time at which stars of different magnitudes will start to saturate the CCD.
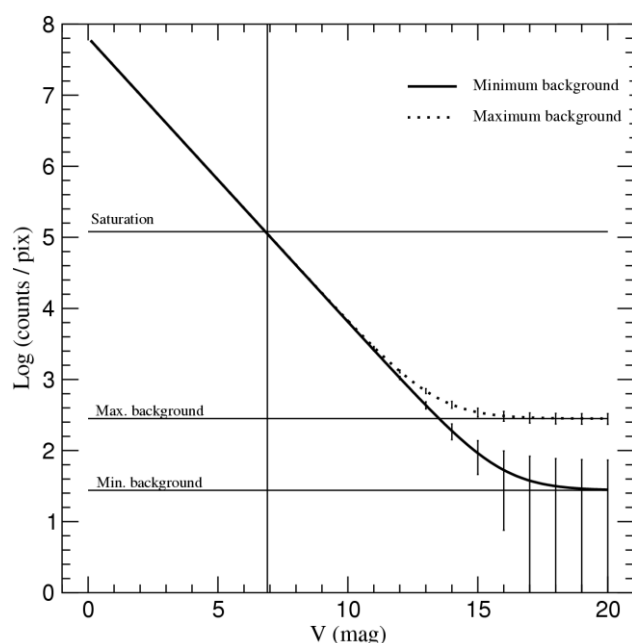

Figure 11: Expected number of counts on the central brightest pixel as a function of V magnitude, for an integration time of 10 s. The error bars correspond to 1σ. The plot also includes the expected background flux computed for maximum and minimum conditions.
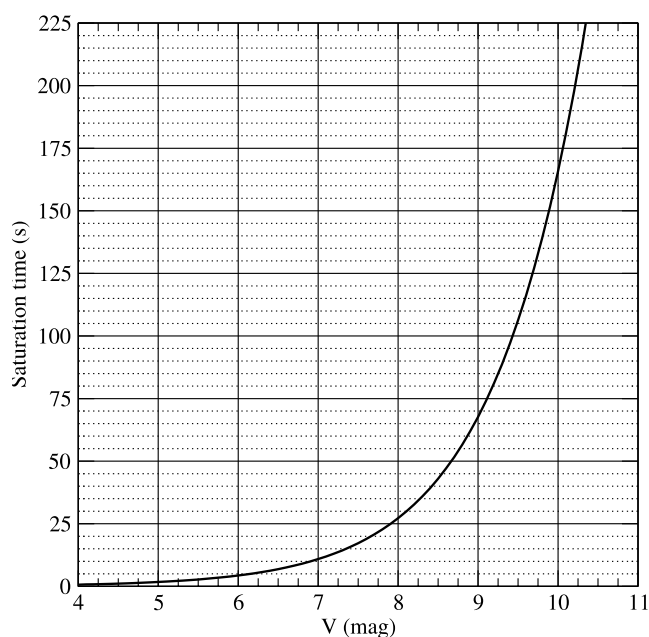

Figure 12: CCD saturation time as a function of V magnitude. Note that for integrations of 50 s, all stars with $m_V < 8.6$ will saturate the CCD. For the shortest OMC integration times (fast monitoring mode: 3 s), the brightest stars that can be observed should be fainter than $m_V > 5$.

4.4 Photometric accuracy

Table 2 shows the expected error (expressed in magnitudes) of a given measurement for various "effective" integration times and magnitudes. "Effective" integration time means the total exposure after combining several shots. The value of 300 seconds corresponds to the "typical effective exposure" obtained by the OSA analysis software using the default parameters. A value around 900 seconds corresponds to the maximum effective exposure one can get in the standard analysis (when changing the default parameters). These values should be used as a guide: they are the best results that can be obtained with the latest version of the analysis software, and they are only valid for isolated stars in "Staring" mode. For an entire 5×5 dither pattern (~2000 s pointing), 900 seconds of effective exposure can also be taken as a representative value.

The values for photometric accuracy have been computed by taking into account the most current knowledge of the OMC instrument. One can see in Table 2 that good photometry can be performed in the V band for objects of quite different brightness. Note that these accuracies can only be obtained for isolated stars for which the background can be properly estimated. Furthermore, in case of dithering the photometric dispersion is >0.02 (magnitudes) in all cases. This value (0.02) is the accuracy of the OMC flat-field matrix. So, if the source is observed in different detector pixels, as occurs for a dithered observation, the accuracy of the flat-field produces an additional scattering on the observed magnitudes of about 0.02 mag.

Table 2: Photometric accuracy (in magnitudes) for different effective exposures and source magnitudes.

source $m_V \rightarrow$	**8**	**10**	**12**	**14**	**16**
effective[2] exposures	assuming a typical background level:				
10s	0.007	0.02	0.1	-	-
300s	-	0.005	0.01	0.045	0.3
900s	-	0.003	0.006	0.026	0.17

---

[2]See Section 4.4 for the definition of an "effective" exposure.

4.5 Focusing

The focusing capabilities of the OMC system depend very slightly on the lens temperature and the pixel location over the detector. The PSF follows a Gaussian distribution whose FWHM remains in the range 1.2 to 1.4 pixels in most cases, as shown in Figure 13.
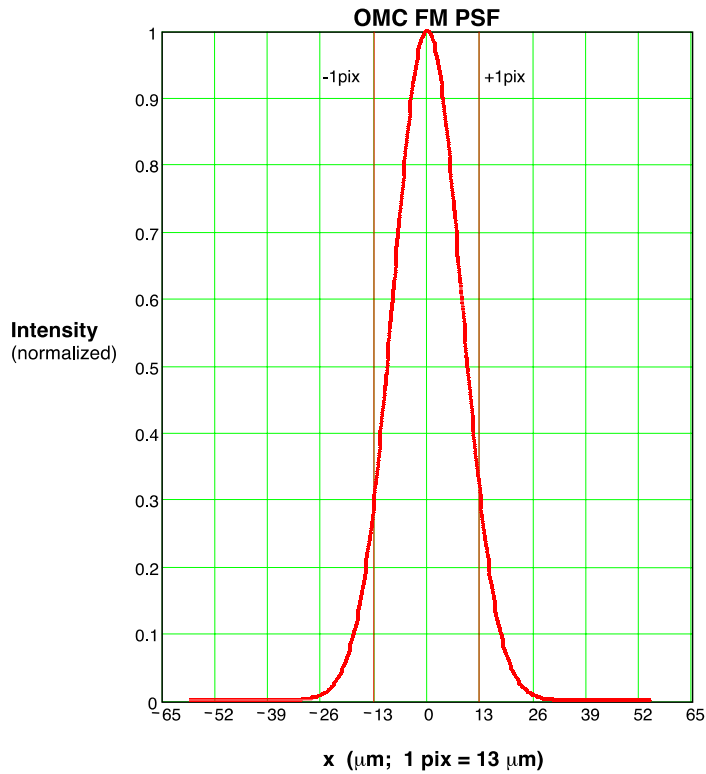

Figure 13: Point Spread Function of the OMC (optical system + detector). The plot shows a fit to the average PSF measured under different conditions. The PSF measured in orbit follows a Gaussian with FWHM ≈ 1.3 pixels. More than 90% of the energy falls within 3×3 pixels.

5   Data products

5.1   Overview of the scientific analysis

A complete description of the data analysis pipelines and modules, as well as the use of the Off-line Scientific Analysis (OSA) software can be found in the OMC Analysis User Manual (see http://www.isdc.unige.ch/integral/analysis). The scientific analysis of all the INTEGRAL instruments is split into a number of steps with similar tasks:

COR - Data Correction

At this step the appropriate calibration data (dark current, bias, flat-field) for the current Science Window are selected and the corrected pixel values for the subsequent analysis are calculated.

GTI - Good Time Handling

At this step Good Time Intervals (GTI) for the current Science Window are derived, based on housekeeping data and attitude information.

IMA - Source Flux Reconstruction and Image Creation

At this step the fluxes of the individual sources are calculated and the source magnitudes are derived. The user can also require building the individual images with the OMC boxes at this step.

Observers will receive the results from all of these steps:

The raw and corrected CCD sub-windows for all pre-defined sources in the field of view. The data are provided in a tabulated format with pixel values as vector entries in a column of the tables. CCD corrected windows will include flat-field calibration, bias and dark current subtraction, but not the removal of cosmic rays.

In addition, a series of tables with derived fluxes and magnitudes for all observed sources as a function of time. By default, photometrical analysis will be performed combining all images obtained within periods of around 10 minutes.

IMA2 - Results Collection

The data concerning one observation are distributed between different files and Science Windows. At this step the OMC flux results are collected into a single table.

The OSA allows the observers to reprocess the OMC data with different parameters as, for example, the sampling time or more recent calibration files. Figures 14-21 show examples of OMC light curves. It can be seen that good photometric results can be obtained for a variety of targets, even with the presence of other sources in the field at relatively small angular distances, as is the case for Cygnus X-1.
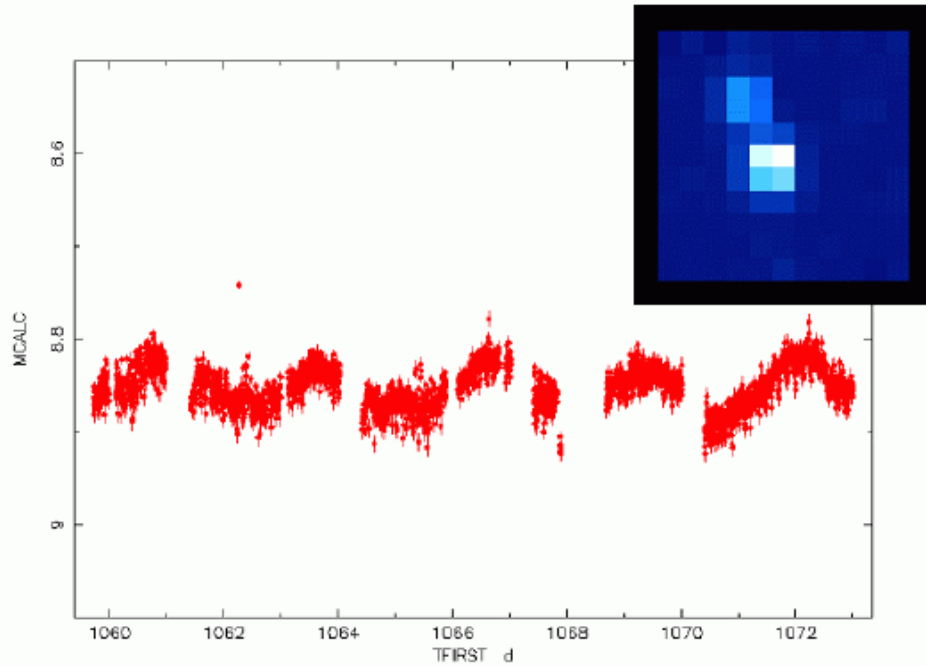
Figure 14: OMC light curve of the high-mass X-ray binary Cygnus X-1 obtained using single exposures of 10 and 30 s. The OMC sub-window for this source is shown on the upper right corner of the graph. Time is in INTEGRAL Julian days. (Credits: OMC Team).
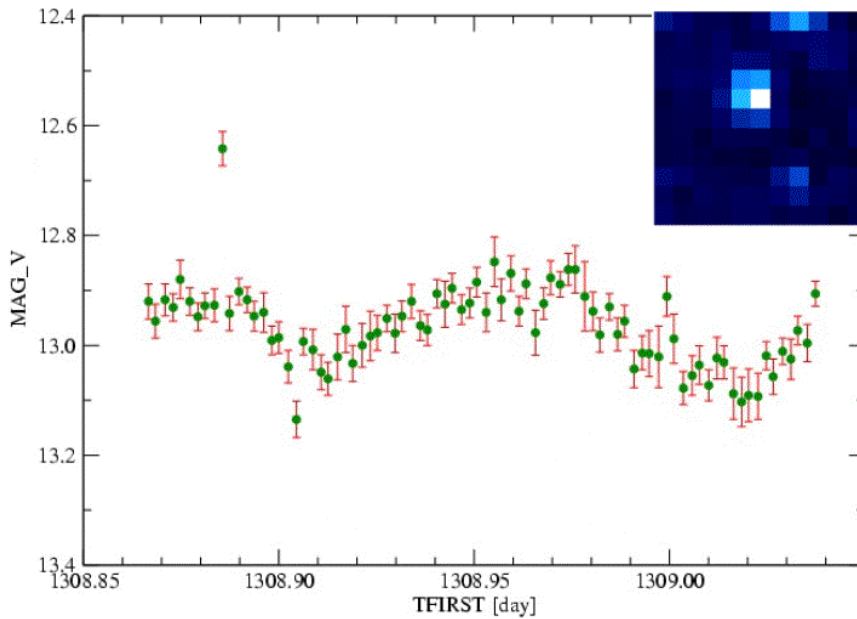

Figure 15: OMC light curve of the low-mass X-ray binary Sco X-1. It is based on single exposures of 100 s. The OMC sub-window for this source is shown on the upper right corner of the graph. Time is in INTEGRAL Julian days. (Credits: OMC Team).
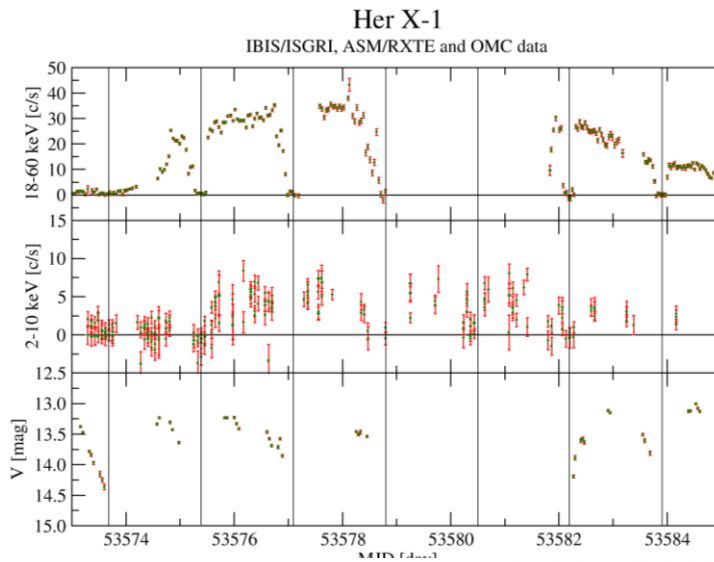
Figure 16: High-energy (RXTE/ASM and INTEGRAL IBIS/ISGRI), and OMC light curves of the low-mass X-ray binary Her X-1 over a period of about 12 days. The orbital period is 1.7 days, marked by vertical lines. X-ray eclipses, when the neutron star is hidden by its companion, are evident. (Credits: OMC Team).
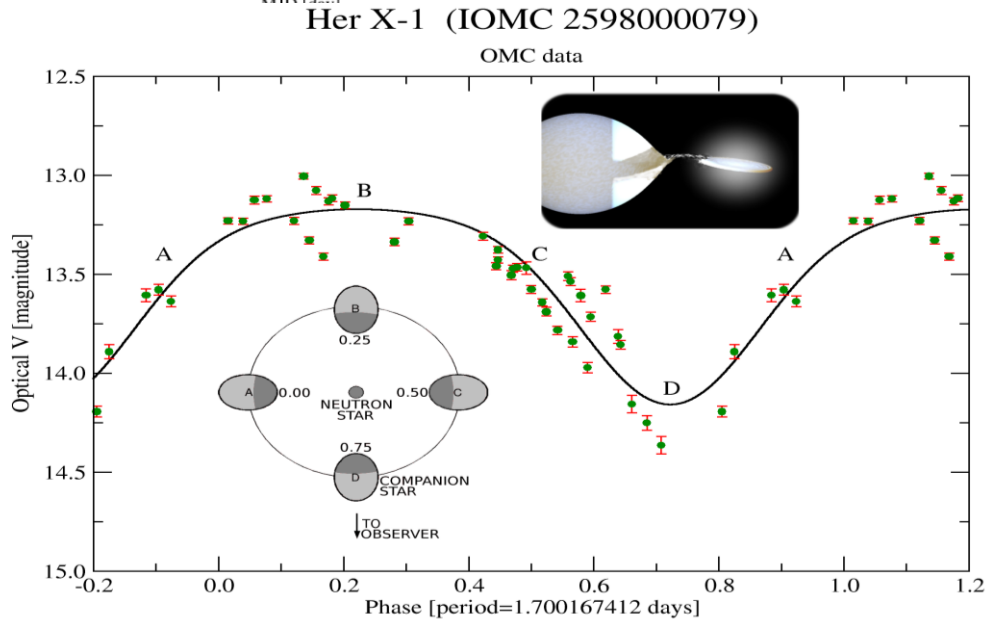

Figure 17: OMC light curve of the low-mass X-ray binary Her X-1 (see Figure 16) folded on the 1.7 days orbital period (Risquez et al. 2008, PoS(Integral08)129). The optical variations are due to the tidal distortion of the companion star, and to the intense X-ray heating of the illuminated face of the companion produced by the neutron star. The insets show an artist's impression of the system (top) and a sketch of the situation at different orbital phases (the orbit is almost circular) - not to scale and omitting the accretion disk (bottom):

- *(A) Orbital phase zero corresponds to maximal radial velocity.*

- *(B) At orbital phase 0.25 one sees the maximum of the optical emission, as one is facing the hot side of the X-ray heated companion.*

- *(D) At orbital phase 0.75 one sees the minimum of the optical emission, as one is facing the cold side of the companion star and the X-ray eclipse.*
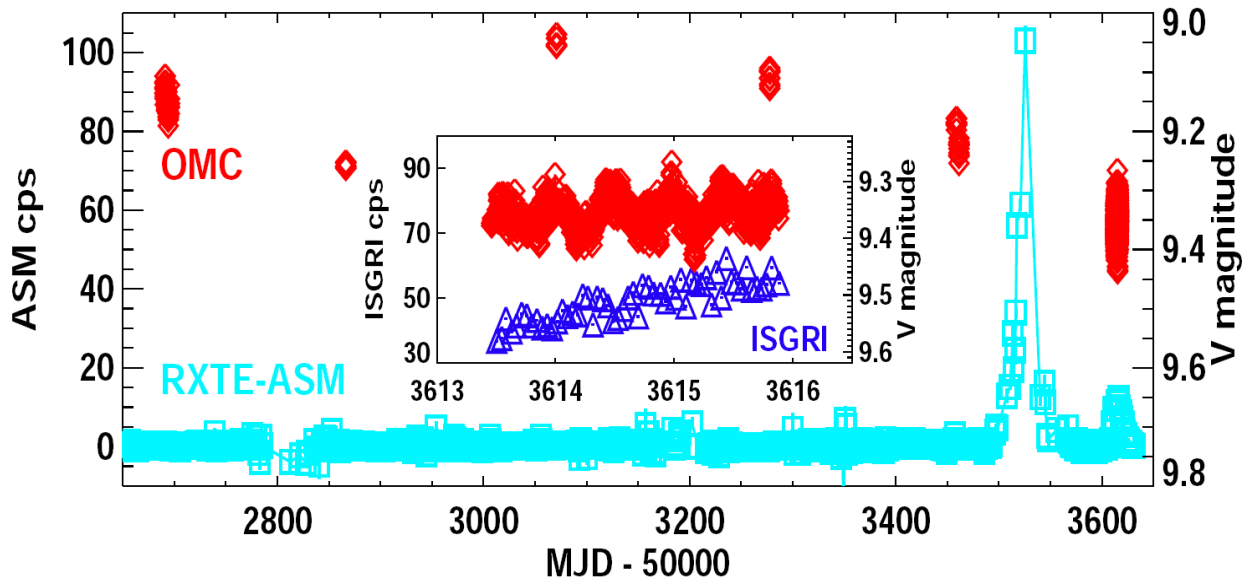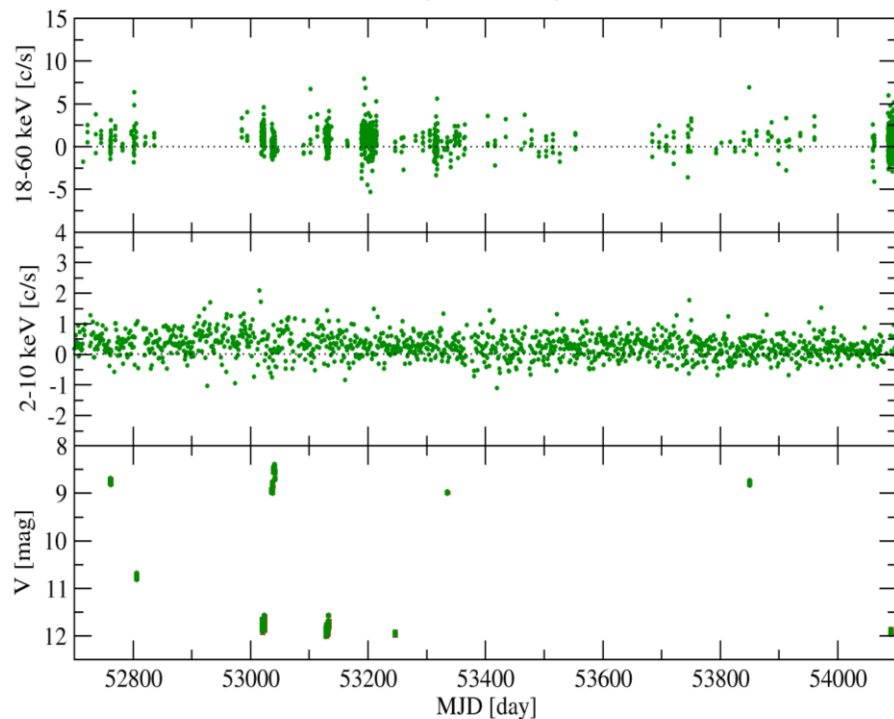
Figure 18: Long-term light curves of the Be/X-ray binary and accreting pulsar 3A0535+262/HD 245770 obtained with the RXTE/ASM (left Y-axis) and the INTEGRAL/OMC (right Y-axis). The inset shows the OMC and ISGRI light curves during the INTEGRAL Target of Opportunity observations around MJD 53613-53616. (Taken from: Kretschmar et al. 2006, ESA SP-604, p. 273).

Figure 19: SS Cygni is a cataclysmic variable (white dwarf with a low-mass donor star) with an orbital period of about 0.275 days. The OMC light curve (bottom panel) shows a strong variability in the optical emission, roughly 40 times in flux. No trends are seen at high energies with the RXTE/ASM and INTEGRAL/IBIS/ISGRI (top panels). (Taken from: Risquez et al. 2008, PoS(Integral08)129).
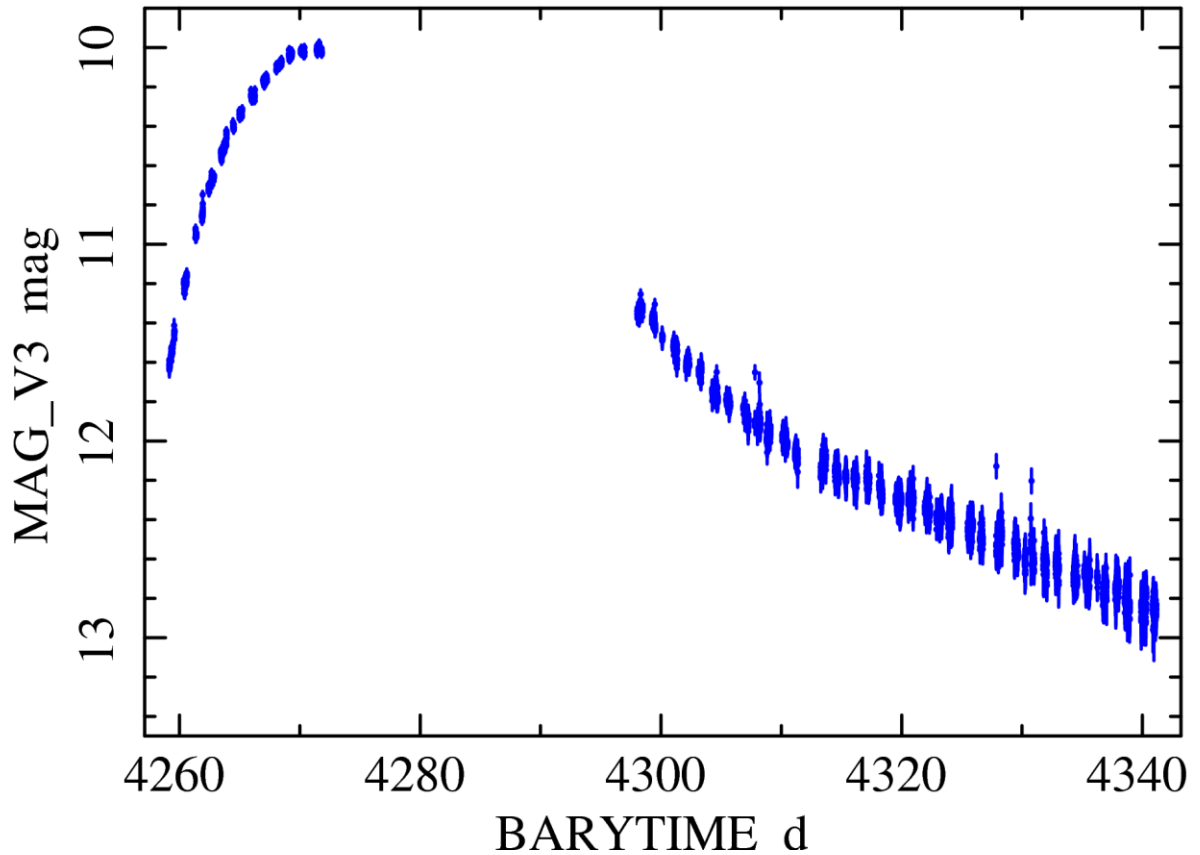
SN 2011fe

Figure 20: OMC light curve of the Type Ia supernova SN2011fe discovered by the Palomar Transient Factory in M101 on August 24th, 2011, a few hours after the explosion. Time is in INTEGRAL Barycentric Julian days. For more details, see Isern et al. 2013, A&A 552, A97. (Credits: OMC Team).
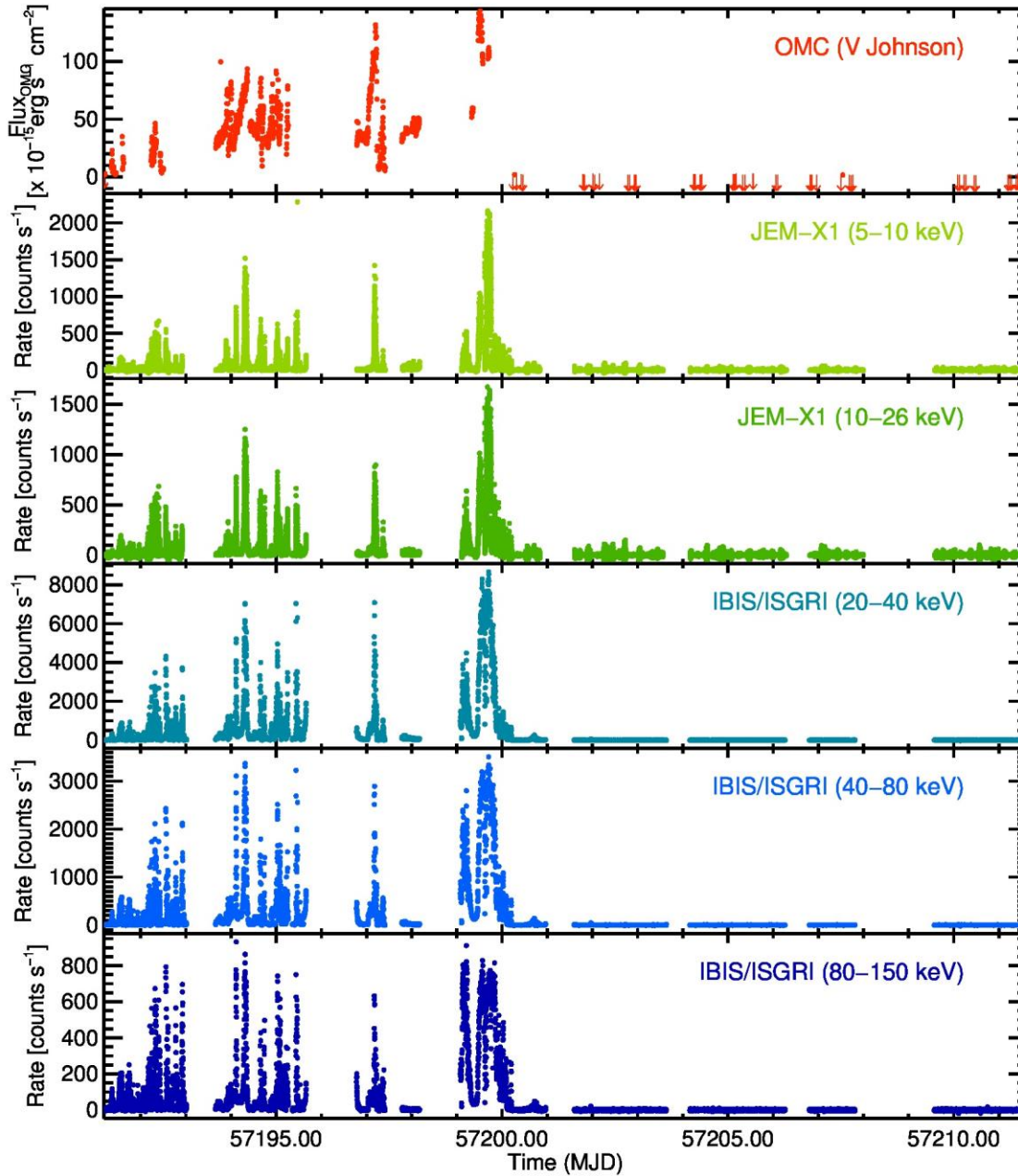
Figure 21: INTEGRAL light curves of the black-hole X-ray transient V404 Cyg (GS 2023+338) during its outburst in June 2015. In quiescence, the V404 Cyg optical V-band emission is dominated by the K star companion, showing a brightness in V of about 17.3 mag. During the outburst in June it reached 11 mag in V, i.e., about 300 times brighter than in quiescence. When comparing the X-ray and optical emission (see J. Rodriguez et al. 2015, A&A 581, L9) some of the optical flares are found to show shapes similar to the high-energy ones, but in other cases there is no clear correlation between high-energy and optical rising/fading. (Credits: OMC Team).

5.2 Known limitations

1. The automatic extraction of fluxes and magnitudes produces reliable results only for point-like sources.

2. If the source coordinates are inaccurate by more than 2 OMC pixels ($\approx 35''$), the analysis software will not be able to re-centre the target and the derived fluxes and magnitudes using the default analysis parameters will not be correct.

3. For extended sources or high-energy sources with large uncertainties in their position, the OMC planning assigns multiple adjacent sub-windows to cover the whole area. In that case, multiple boxes are found with different ranks but with the same OMC_ID.

    [Note that from OSA 6.0 onwards these mosaics of sub-windows can be correctly analysed by using IMA_wcsFlag=yes (default in current OSA), once the coordinates are well defined (e.g., from X-ray observations). In this case, o_src_get_fluxes creates a virtual 11×11 pixel sub-window inside the whole area centred at the source position given in the OMC Input Catalogue. After that, OSA works on this new sub-window and ignores the previous windows of the mosaic. This is an internal software trick; these virtual sub-windows do not exist as standard sub-windows (o_ima_build, for example, will not create these virtual sub-windows as images of 11×11 pixels). Note that with IMA_wcsFlag=no, these mosaics of sub-windows will not be analysed correctly as the software treats each box individually. Users should also note that even with IMA_wcsFlag=yes, for those new sources which are not yet included in the OMC Input Catalogue, these virtual sub-windows cannot be created because the software extracts the coordinates from the OMC Input Catalogue. In addition to this method, the observer may extract the optical photometry manually from the corrected images produced by the analysis pipeline. As examples, Figure 4 shows the single OMC sub-window generated for a point source with precise coordinates like Cygnus X-1, while Figure 5 displays a mosaic of 5×5 OMC sub-windows generated for the High Mass X-ray Binary 4U 1901+03 which has no accurate coordinates.]

4. If another star is within a few pixels from the source of interest, it can introduce systematic errors in the derived fluxes and magnitudes. The strength of this effect can be different for different pointings, since the relative position in the sub-windows will change slightly for different rotation angles.

5. Some of the bright sources slightly saturating one or a few pixels might not be detected as saturated sources. As a consequence, their derived magnitudes may not be correctly computed. The observer should check in Figure 12 whether the source could be saturating the CCD for a given integration time, and re-analyse the data rejecting the shots with the longest integration times.

6. Due to thermo-elastic deformations, the alignment of the OMC optical axis with the spacecraft attitude reference (after correcting for the known OMC misalignment) may diverge by up to $30''$ (≈ 2 pixels). This is corrected for in the analysis (OSA 5 upwards) using the photometric reference stars, giving an accuracy of $\leq 2''$ in most cases.